UCN Cryo Memo

Takahiro OKAMURA

August 8, 2018

Contents

Chapter 1

Heat Transfer of He-II

1.1 Boiling curve of He-I and He-II

1.1.1 In case of ordinary viscous fluid

This subsection is not a main topic. Please skip this section if you know boiling curve, nucleate boiling and film boiling.

Figure 1.1 shows the heat transfer curve (boiling curve) of ordinary viscous fluid [1]. Vertical axis is heat flux from the heater (W/m^2). Horizontal axis is temperature difference between heated surface temperature and saturated temperature. As shown in the figure, there are three regime as follows.

- non boiling region = natural convection regime (Region I)
- nucleate boiling regime (Region II)
- film boiling regime (Region III)

In general, there are two type of boiling. One is nucleate boiling. Another is film boiling. According to the boiling curve so called Nukiyama's boiling curve [2][3] for the ordinary viscous fluid, nucleate boiling enhances the heat transfer coefficient due to buoyancy of a lot of nucleate bubbles and there are both gas and liquid phase on the heated surface. But on the contrary, in case of film boiling, continuous vapour layer covers the heater. If current heating is employed, heated surface temperature is drastically increasing from point C to point E without going through point D. This means that the heat transfer characteristics of the film boiling is not good compared to nucleate boiling heat transfer due to the existence of continuous film layer contacting the heated surface (no liquid phase on the surface of the heater). **Heat flux which transits from nucleate boiling to film boiling (point C) is defined as critical heat flux (CHF) for the classical viscous fluid[1]. Concerning the "CHF", we have to pay attention to the definition difference between classical viscous**

[1]In this paper, critical heat flux is expressed by q_{cr}.

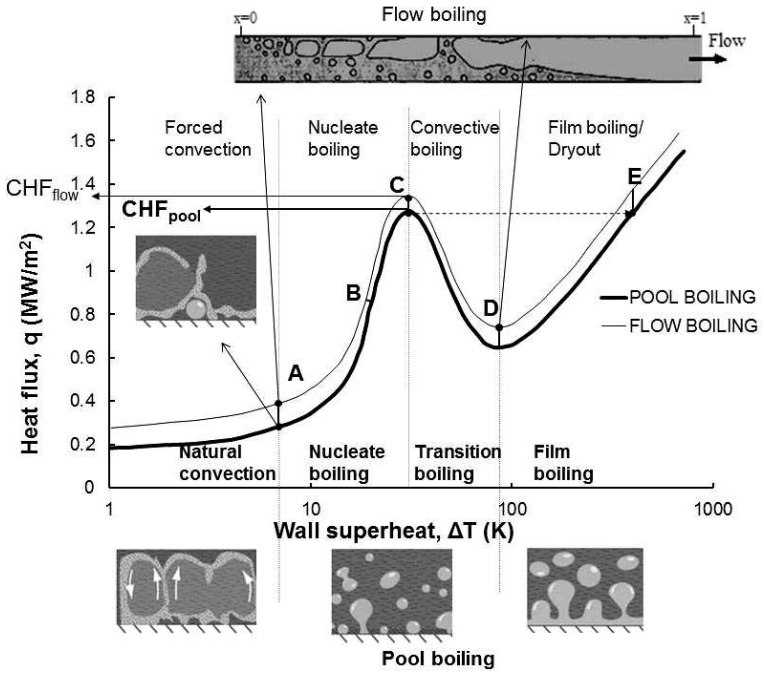

Figure 1.1: Boiling curve for viscous classical fluid [1].

fluid and superfluid helium. In case of superfluid helium, critical heat flux is defined as the point at which film boiling begins to occur on the heated surface (see section 1.1.2).

Boiling curve example for the pressurized He-I was shown in the figure 1.2. Since He-I is normal viscous fluid, the boiling curve is almost same tendency as figure 1.1. Once heat flux exceeds CHF, q_{cr}, heated surface temperature is drastically increased (jumped) [2] and film boiling heat transfer regime is observed.

1.1.2 In case of He-II

Pressurized He-II and Satureted He-II

Following two kinds of boiling curve should be considered in case of He-II.

- Boiling curve in case of **"Pressurized helium"**
- Boiling curve in case of **"Saturated helium"** [3]

[2]The heater is covered by the vapour film without no liquid phase. Vapour film shape is basically governed by Rayleigh-Taylor instability.

[3]The thermo physical point of the saturated He-II shown in the figure 1.3 is not on the SVP. Important thing is that the heated surface area is a little bit subcooled due to the existence of hydrostatic pressure head (immersion depth). If the heated surface is located very close to the gas-liquid interface of saturated He-II, the thermo physical condition is almost on the SVP line. Detail about them is introduced in the section 1.2.2.

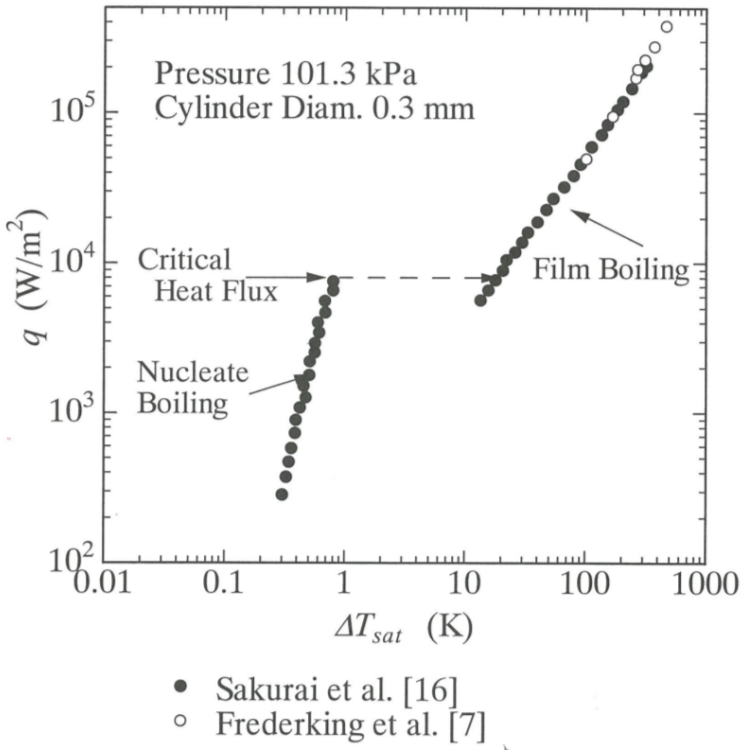

Figure 1.2: Boiling curve example for He-I.

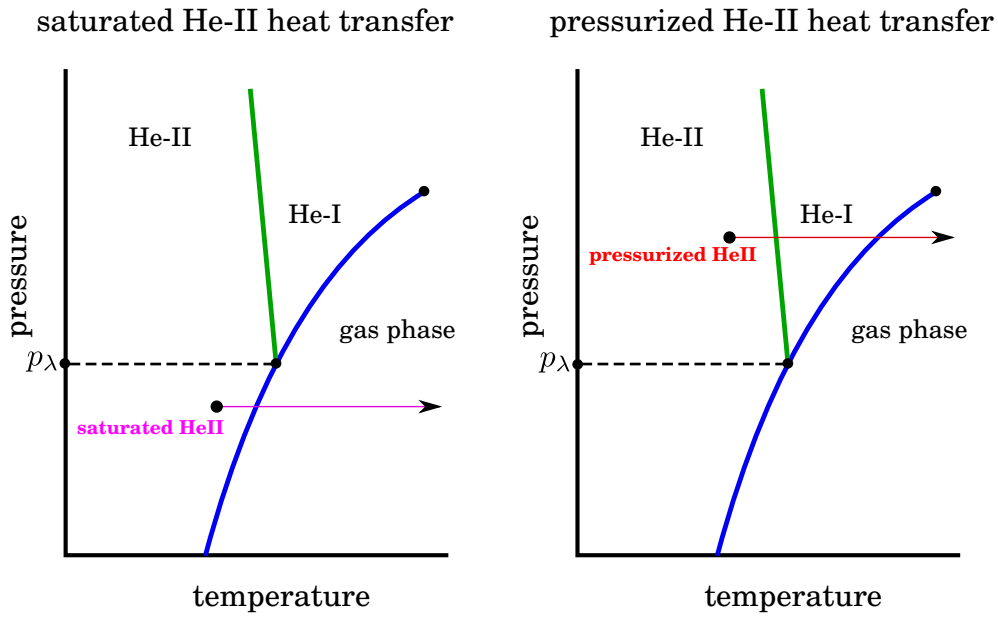

Figure 1.3: Thermo physical condition difference between saturated He-II and pressurized He-II.

Figure 1.3 shows the hermo physical condition difference between saturated He-II and pressurized He-II. Main difference between above two thermo physical state is as follows.

- **Pressurized He-II :**
  System pressure is larger than lambda pressure, $p_{sys} > p_\lambda$. Therefore the He-I phase is appeared partially (see right side of the figure 1.3.)

- **Saturated He-II :**
  System pressure is less than lambda pressure, $p_{sys} < p_\lambda$. Therefore, He-I phase never appears. (see left side of the figure 1.3.)

where, lambda pressure, $p_\lambda \sim 5$ kPa. **In the UCN, the thermo physical condition of IPHe-II can be regarded as "Saturated He-II".**

Boiling curves

Figure 1.4 shows the heat transfer curve in case of saturated He-II and pressurized He-II measured by M. Shiotsu *et. al.* Vartical axis indicates heat flux from the heated surface. Horizontal axis is temperature difference between heated surface temperature[4] and bath temperature. There are two regimes as follows (see figure 1.4.)

- Non boiling regime. (Region I)
- Film boiling regime. (Region II)

There is no "nucleate boiling regime". It is main difference between ordinary viscous fluid and superfluid helium. Non boiling regime is superfluid single phase flow regime. Actually, this regime is mainly determined by Kapitza conductance. q_{cr} indicates critical heat flux for the saturated and pressurized He-II. **The definition of q_{cr} in case of He-II is the heat flux when the helium contacting the surface of the heater transits from superfluid to normal fluid (He-I) or helium gas.** [5] Therefore, if the heat flux is less than critical heat flux, q_{cr}, helium in the dewar can be regarded as a superfluid single phase state. If the heat flux exceeds q_{cr}, helium adjacent to the heater becomes gas phase. **It is necessary to be aware that the behavior of temperature rise of the film boiling layer is decisively different between saturated He-II and pressurized He-II. Next subsection introduces this difference.**

[4]The heated surface temperature is not a He-II temperature but a heated surface temperature (=temperature of the solid including Kapitza conductance).

[5]In case of saturated He-II, He-II adjacent to the heater transits to helium gas according to the phase diagram (see figure 1.3). In case of pressurized He-II, He-I is once appeared, however the heat transfer characteristics of liquid He-I itself (natural convective heat transfer of He-I) is much lower than that of the He-II. Therefore soon after that heated surface is covered by gas phase. (see schematic image of **c)** shown in the figure 1.8).

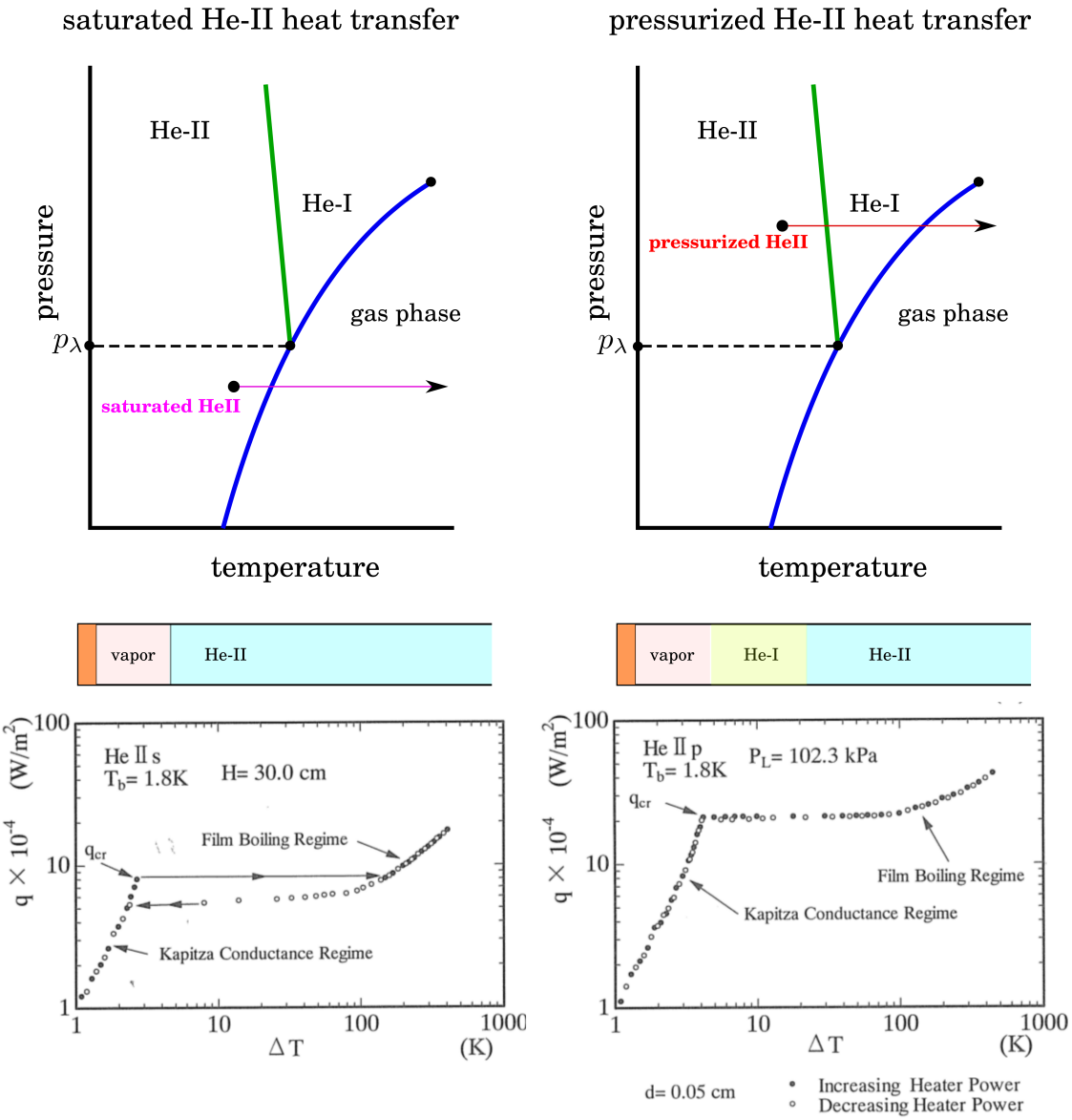

Figure 1.4: Typical boiling curve for pressurized and saturated He-II. He IIs and He IIp in the figure mean initial of "Saturated" and "Pressurized" He-II, respectively. $H = 30.0$ cm means the hydrostatic pressure head in case of saturated He-II.

1.1.3 Boiling curve difference between "saturated He-II" and "pressurized He-II"

Figure 1.5 shows the schematic boiling curves for the **saturated He-II** and **pressurized He-II**, respectively. This schematic pictures are drawn based on observed boiling curves introduced in the figure 1.4. Main difference between them is that

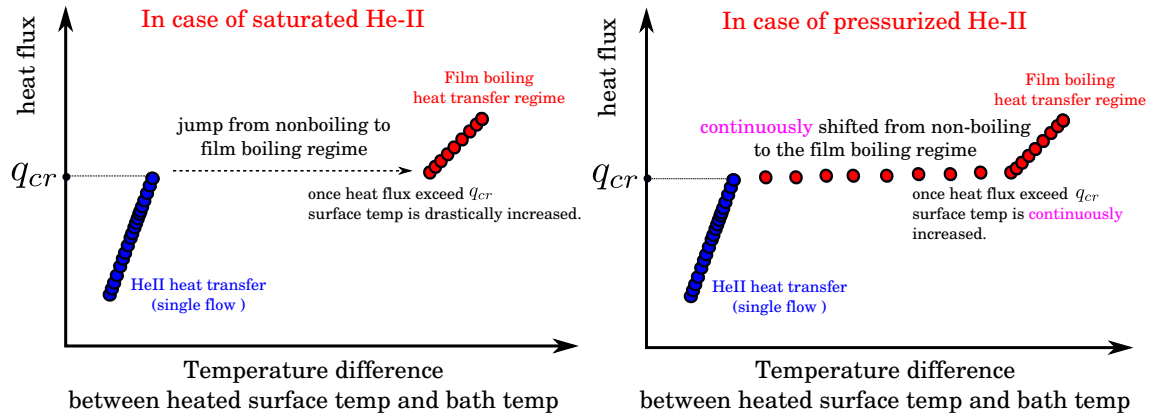

Figure 1.5: Boiling curve difference between saturated He-II and pressurized He-II.

- **In case of "saturated He-II", the heated surface temperature adjacent to the heat source is drastically increased (jumped) to the film boiling regime (jump to more than 100 K).** [a]
- In case of "pressurized He-II", the heated surface temperature is continuously increased to the film boiling regime step by step.

[a] see left-bottom figure in the figure 1.4 and left side of figure 1.5.

Therefore, in the UCN case, since thermo physical state of IPHe-II is saturated He-II, helium adjacent to the heated surface[6] becomes transits to the gas phase and its temperature is drastically increased (jumped) to the film boiling temperature regime as shown in the figure 1.5 even though a little bit larger heat flux than critical heat flux, $q \sim q_{cr}$, is added to the IPHe-II.

In addition, as the hydrostatic pressure head decreases, the critical heat flux tends to decrease as well. (see section 1.2.3) That is, in the case of saturated He-II, film boiling tends to occur when the hydrostatic pressure head is small. That is, film boiling occurs with a slight heat flux. Once gas phase appears in the He-II, its temperature is drastically higher than bath temperature.

Therefore, we have to clarify where is the heat source and we have to clarify critical heat flux in the UCN. Actually, in the UCN case, quantitative evaluation for the location of heat source and critical heat flux is non-trivial because one of the heat source can be regarded as **volumetric heating, Q_{vol}.** Heat source and some difficulties are introduced in the next subsection.

[6] We have to clarify what and where is the heat source in the UCN case.

1.1.4 Importance of CHF and heat source

According to the boiling curve characteristics of saturated He-II, following two items should be considered.

- **Critical heat flux (CHF)**, q_{cr}, should be considered. In case of saturated He-II, critical heat flux strongly depends on hydrostatic pressure head. For example, shallow hydrostatic pressure head leads smaller critical heat flux. This means that it is easy to be transition to film boiling with high temperature in case of shallow hydrostatic pressure head. (see section 1.2.3)
- **Heat input distribution (where is the heat source)** should be considered. UCN system is non-trivial. There are mainly two heat source in the UCN IPHe-II system.
  - **source-1:** heating from the IPHe-II chamber wall, Q_{wall}.
  - **source-2:** volumetric heat source. (non-trivial term), Q_{vol}.

  Total Heat deposit, Q_{tot}, is roughly approximated as follows.

$$Q_{tot} = Q_{wall} + Q_{vol} \tag{1.1}$$

Figure 1.6 is the image of source-1 and source-2 and influence of these two-sources. As shown in the figure, Q_{wall} is heat source from the UCN dewar wall and it is trivial heat source. We can evaluate critical heat flux and predict flow behaviour of two phase field due to the film boiling[7]. There are a lot of experimental results on the boiling curve for the wall heating case. In such a case, film layer is covered on the heater surface after exceeding critical heat flux (CHF). In this case, the inner wall of the UCN bottle is covered by film vapour phase. Therefore, film vapour phase generated on the heated surface can be regarded as a kind of insulation. So there may be no problem from the view point of keeping IPHe-II temperature constant.

On the contrary, Q_{vol} is volumetric heating term which is the heat generation rate due to the directly neutron injection into the He-II. In this case, there are no boundary (solid wall) and there are no experimental data on boiling curve and directly optical observation when the heat source exceed critical heat flux. In the former case, critical heat flux can be easily evaluated by using Gorter-Mellink equation, however in the later case, it is quite difficult to evaluate critical heat flux because it is difficult to obtain the information about effective cross sectional area, A_{eff} for the heat generation region. This means that it is difficult to evaluate heat flux for the volumetric heating, $q_{vol} = Q_{vol}/A_{eff}$.

[7]The heat flux based on the Q_{wall} is very small in the case of UCN because of the large surface area of the UCN bottle. If sligh hydrostatic pressure head such as several cm exists in the UCN bottle, the heat flux based on the Q_{wall} is smaller than q_{cr}.

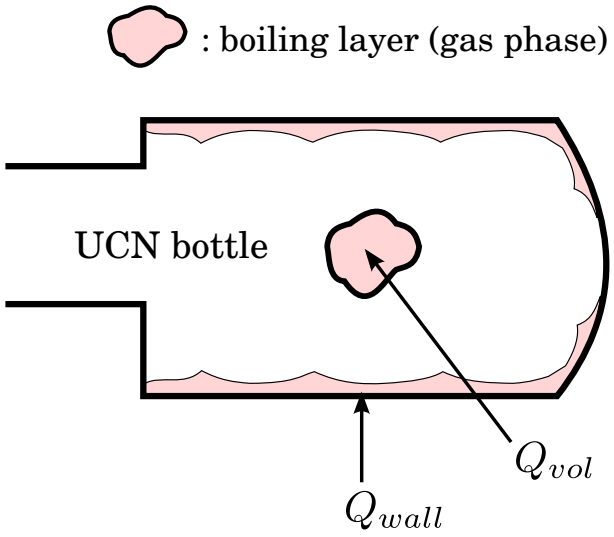

$$Q_{tot} \simeq Q_{wall} + Q_{vol}$$

Figure 1.6: Schematic image of flow field due to the heat input of $Q_{tot} = Q_{wall} + Q_{vol}$ in IPHe-II bath if the heat input exceed CHF.

1.1.5 Boiling behaviour due to the volumetric heating ??

Actually, it is quite difficult to image a picture of the boiling behaviour in the case of the volumetric heating which is higher value than a CHF. This is because nucleate boiling (a kind of bubble) does not occurs in the He-II bath due to superfluidity such as quite high thermal conductivity which inhibits to generation of hot spot that can become a origin of the nucleate boiling.

But if the volumetric heating whose power is higher than a certain value (CHF) is added to the He-II bath as shown in the schematic figure 1.6, gas phase like film boiling may be appeared. So the density of the appeared gas phase is dilute compared to the liquid He-II bulk. As a result, neutron does not interact with gas phase with low density. After that the neutron interacts with next liquid He-II region and instead of creating new vapour layer, the original vapour phase shrinks into a liquid He-II. Therefore probably, the location of the gas phase does not keep constant point. This means that the gas phase is fluctuated around a certain point which is most probable point of neutron injection. Anyway, the temperature of the gas phase may also have a possibility to increase drastically as shown in the left figure of figure 1.5 (boiling curve for the saturated He-II). If the small hydrostatic pressure head, such kind of boiling phenomenon with high temperature gas phase is likely to appear due to the volumetric heating, Q_{vol}.

The appearance of the gas phase (film boiling regime) is basically described in the field of nucleation theory. According to the thoery, there are two machanism on the appearance of the boiling phenomenon.

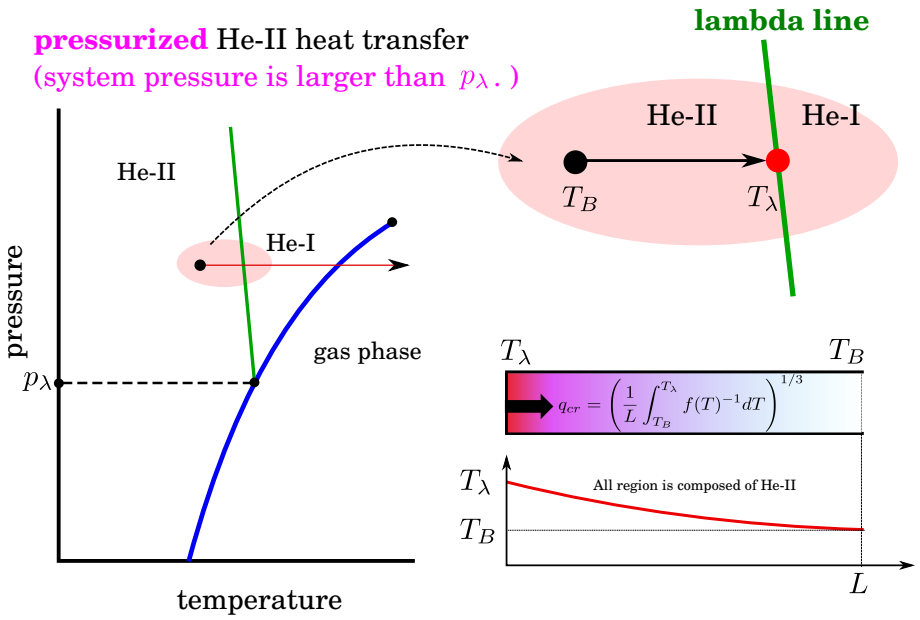

Figure 1.7: Schematic image of $p-T$ phase diagram and flow field when reaching CHF.

- Heterogeneous nucleation
- Spontaneous nucleation

In the UCN case, IPHe-II has a high purity (quite low contamination). Therefore, the appearance of the boiling due to the volumetric heating may be mainly based on the spontaneous nucleation. Probably, nucleation mechanism of He-II due to the volumetric heating based on the neutron injection seems to be one of the unsolved fields and worth studying.

1.2 Critical Heat Flux

In case of saturated He-II, Once gas phase appears near the heat source, its temperature may increase drastically even though a little bit higher heat input than CHF. If you don't permit to the appearance of the high temperature gas region, we have to design the system such that the film boiling does not appears in the IPHe-II bulk. It is easy to do so in case of pressurized He-II, however it is a little bit taking care of hydrostatic pressure head in the case of the saturated He-II.

In the next subsection, critical heat flux (CHF) is considered in case of pressurized He-II and saturated He-II by referring $p-T$ phase diagram of ^{4}He.

1.2.1 CHF in case of pressurized He-II

Figure 1.7 shows the phase diagram and temperature distribution at $q = q_{cr}$. If the heater power gradually increases, heated surface temperature and He-II temperature

contacting the heated surface also increase gradually. When He-II temperature contacting the heater reaches the lambda temperature, the heat flux from the heater at this moment is defined as critical heat flux. The thermo-fluid behaviour until reaching the critical heat flux is in the non-boiling state, and heat transport by the counter flow is carried out. Therefore following Gorter-Mellink equation is satisfied when heat flux reaches critical heat flux, $q = q_{cr}$.

$$q_{cr} = \left(\frac{1}{L} \int_{T_B}^{T_\lambda} f(T)^{-1} dT \right)^{1/3} \tag{1.2}$$

The critical heat flux, q_{cr} is determined by

- system dimension (in this example, system length = L.)
- integral of $f(T)^{-1}$ from bath temperature, T_B, to lambda temperature, T_λ.

If the bath temperature is constant, the critical heat flux is almost independent of the system pressure, because the lambda temperature is almost constant [8], Therefore the integral value of $f(T)^{-1}$ is also constant for the system pressure change.

Figure 1.8 shows the schematic boiling curve and flow behaviour for the non-boiling region, CHF and film boiling region.

- non-boiling regime: There is a temperature gap between heated surface temperature and He-II temperature contacting the heater due to the Kapitza conductance.
- film boiling regime: The temperature of the film layer is much higher than lambda temperature, therefore Kapitza conductance is disappeared between heated surface and gas phase. This means that the heated surface temperature is almost equal to the gas temperature contacting the heater.

1.2.2 CHF in case of saturated He-II

Figure 1.9 shows the $p - T$ phase diagram of saturated He-II with and without hydrostatic pressure head.

In case of no hydrostatic pressure head, ($\Delta p = \rho g H = 0$).

The thermo phsycal condition near the heater is on the SVP line shown in the left side of figure 1.9. Therefore the He-II temperature without heat input is almost equal to the saturated temperature (not subcooled). Ideally speaking there is no temperature difference between saturated temperature and heated surface temperature when the

[8] actually, lambda line is slightly inclined with respect to the vertical direction. So the lambda temperature changes slightly with respect to system pressure.

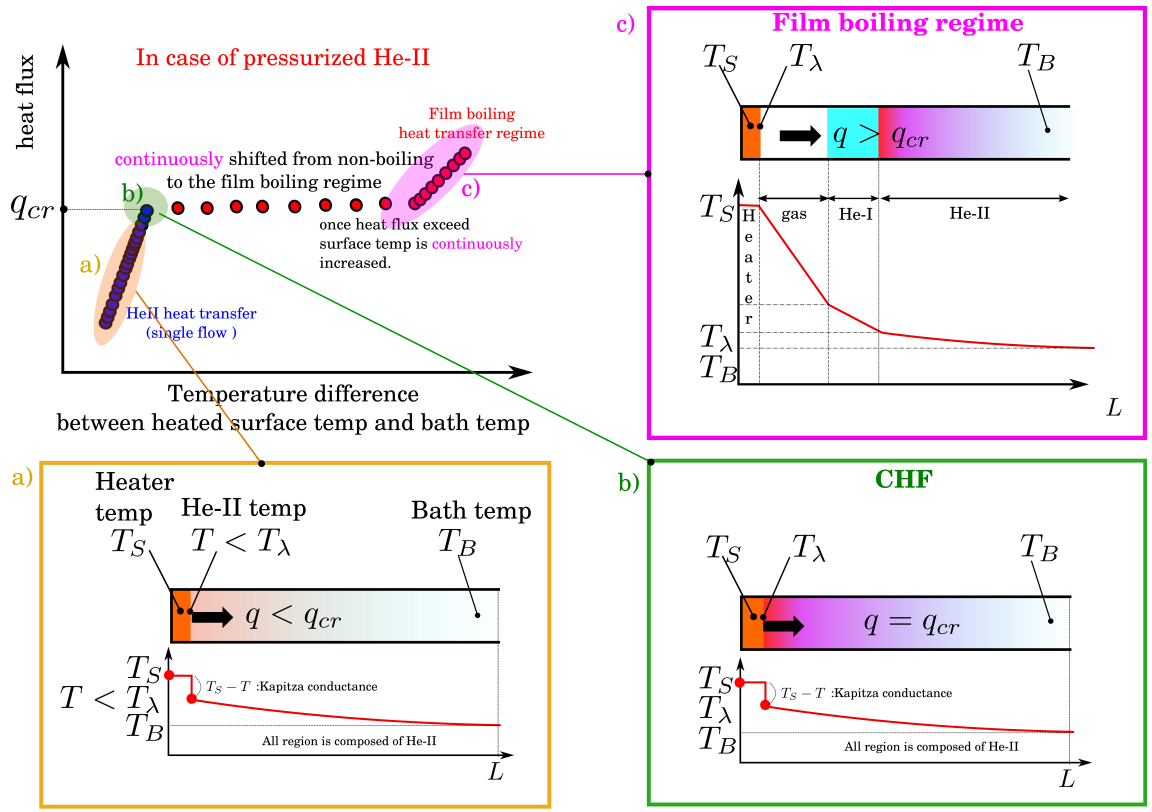

Figure 1.8: Schematic image of boiling curve and corresponding flow field in the **pressurized** He-II for the non boiling regime (Kapitza conductance regime), CHF and film boiling regime.

heater is turned on. In such a case, critical heat flux, q_{cr} for the Gorter-Mellink naive duct with the length of L is described as follows.

$$q_{cr} = \left(\frac{1}{L} \int_{T_{sat}}^{T_{sat}} f(T)^{-1} dT \right)^{1/3} \simeq 0 \tag{1.3}$$

There is no temperature difference for the integral of the $f(T)^{-1}$. This means that even thought the injection of infinitesimal heat into the He-II ($q = \epsilon$), boiling phenomenon occurs because $q = \epsilon > q_{cr} \simeq 0$. In addition, according to the boiling curve of the saturated He-II (see left side of the figure 1.5), the gas phase temperature is jumped and much higher than saturated vapour pressure, T_{sat} mainly due to the volumetric heating term, Q_{vol}. Probably such a gas phase with very high temperature domain may reduce UCN production efficiency.

In case of finite hydrostatic pressure head, ($\Delta p = \rho g H \neq 0$).

If there is some hydrostatic pressure head shown in the right side of the figure 1.9, the themo physical condition is a little bit difference in the case of the no hydrostatic pressure head. The thermo physical conditions in the right side of the figure 1.9 are as follows.

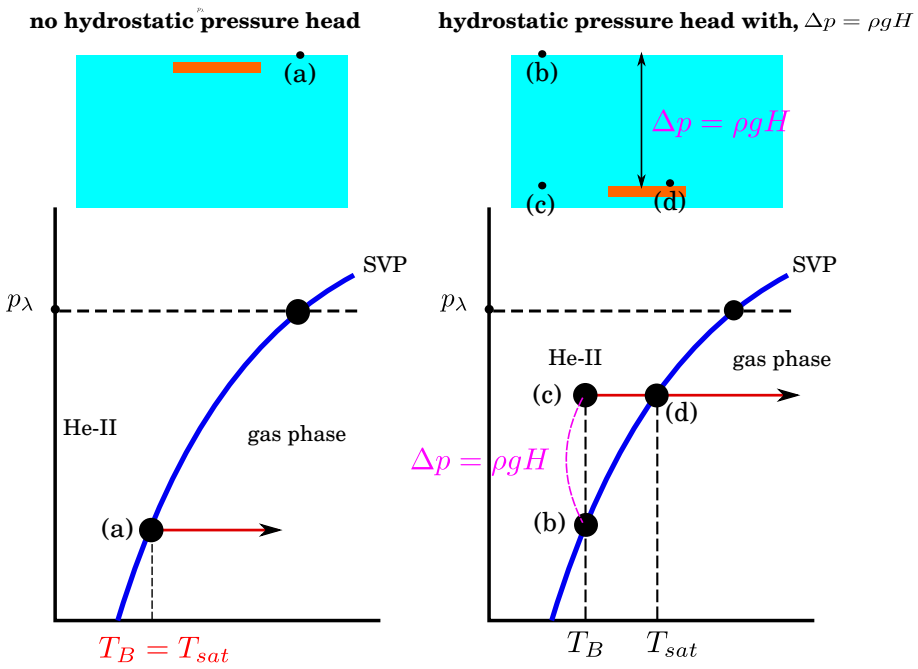

Figure 1.9: Schematic image and $p - T$ phase diagram in the case of w/ and w/o hydrostatic pressure head (immersion depth).

- point (b): gas-liquid interface
- point (c): far from the heated surface with $\Delta p = \rho g H$.
- point (d): surface temperature with $\Delta p = \rho g H$ when film biling begins.

Therefore in case of Gorter-Mellink naive duct with the length of L, the critical heat flux, q_{cr}, with finite hydrostatic pressure head, $\Delta p = \rho g H \neq 0$ is described by

$$q_{cr} = \left(\frac{1}{L} \int_{T_B}^{T_{sat}} f(T)^{-1} dT \right)^{1/3} \gg 0 \tag{1.4}$$

Unlike when the hydrostatic pressure head is zero, the critical heat flux has a finite value, ($q_{cr} \gg 0$). Therefore the film boiling does not occur even though a relatively large heat flux is applied to the He-II bath in the case of the $\Delta p = \rho g H \neq 0$. This means that when the heat flux, q, is smaller than CHF, $q < q_{cr} \gg 0$, He-II for the all region keeps superfluidity (liquid phase). And the value of the critical heat flux, q_{cr}, can be adjusted by changing the hydrostatic pressure head. As shown in the right side of the figure 1.9, the deeper hydrostatic pressure head, the larger the critical heat flux, q_{cr} because the gradient of the SVP is positive (see next subsection 1.2.3.). This tendency were observed from various experimental results. Next subsection shows the relationship between critical heat flux and hydrostatic pressure head (see subsection 1.2.3.).

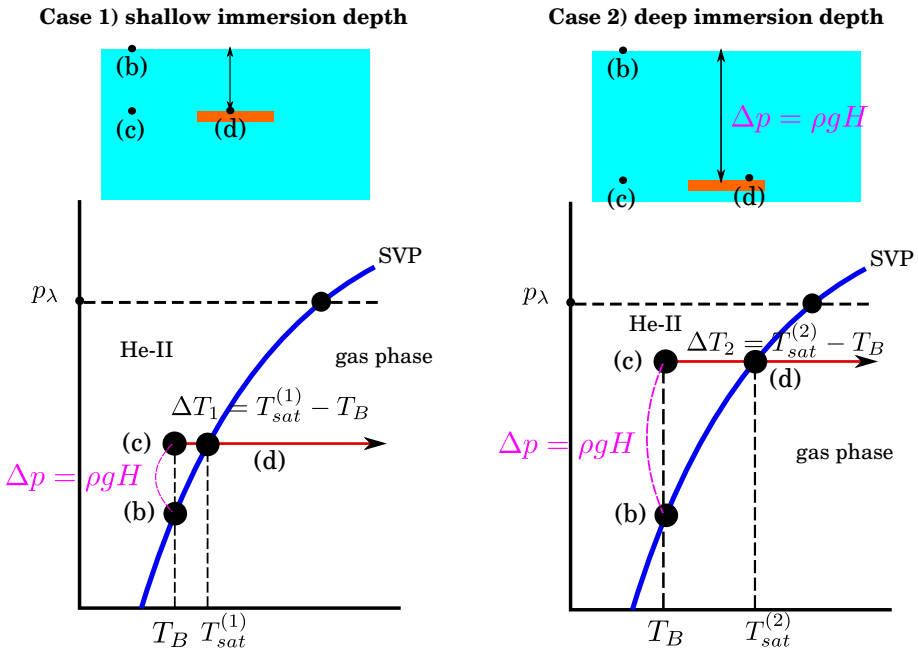

Figure 1.10: Schematic image and $p-T$ phase diagram in the case of shallow immersion depth and deep immersion depth.

1.2.3 Critical Heat Flux vs Hydrostatic Pressure Head

Qualitative evaluation

Figure 1.10 shows the schematic image and $p-T$ diagram for following two cases. Case 1 and Case 2 in the figure 1.10 show the shallow and deep hydrostatic pressure head. We consider the temperature difference between bath temperature and saturated temperature, $\Delta T = T_{sat} - T_B$. Each temperature difference is

$$\Delta T_1 = T_{sat}^{(1)} - T_B, \quad \text{(case-1)} \tag{1.5}$$

$$\Delta T_2 = T_{sat}^{(2)} - T_B, \quad \text{(case-2)} \tag{1.6}$$

Obviously, deeper hydrostatic pressure head becomes large temperature difference ΔT.

$$\Delta T_2 > \Delta T_1 \tag{1.7}$$

Therefore the integral of the $f(T)^{-1}$ in case of case-2 is larger than that in case of case-1.

$$\int_{T_B}^{T_{sat}^{(2)}} f(T)^{-1} dT > \int_{T_B}^{T_{sat}^{(1)}} f(T)^{-1} dT \tag{1.8}$$

Therefore according to the equation (1.4), the critical heat flux in case of case-2 is larger than case-1.

$$q_{cr}^{(2)} > q_{cr}^{(1)} \tag{1.9}$$

Next experimental results for the relation between CHF and hydrostatic pressure head is introduced.

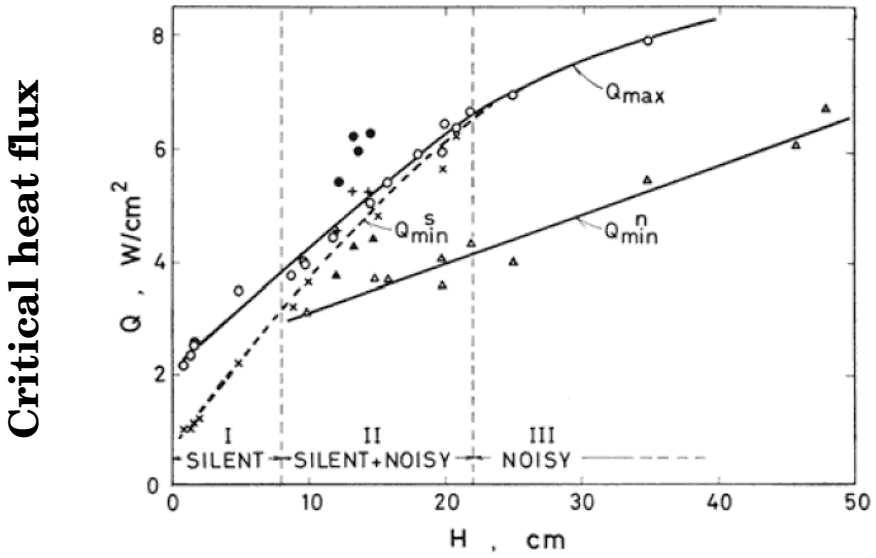

Fig. 2. Critical heat fluxes as a function of the immersion depth at T_b = 1.91 K in saturated helium-II. Solid points represent data obtained on the thin frost-covered surface.

Advances in cryogenic engineering, Vol.25, p-374

Figure 1.11: Relationship between critical heat flux and hydrostatic pressure head (immersion depth) [4].

Experimental results

Figure 1.11 shows the experimental results example on the relationship between critical heat flux and hydrostatic pressure head [4]. Vertical axis and horizontal axis is the critical heat flux and hydrostatic pressure head (immersion depth), respectively. "SILENT", "SILENT+NOISY" and "NOISY" in the figure means the behaviour of the film boiling after reaching the CHF and now we can neglect these technical words. As shown in the figure, smaller immersion depth induces low critical heat flux. This tendency is consistent with qualitative evaluation described above. **Actually, sicne critical heat flux strongly depends on the shape and dimension of the channel and heater, the practical critical heat fluxes and immpersion depth shown in the figure can not be beneficent in the UCN case. But we have to take into account of the relationship between CHF and immersion depth in addition to the temperature jump behaviour observed after reaching CHF in the case of the saturated He-II.**

1.3 Required Hydrostatic Pressure Head in the UCN-bottle

Required hydrostatic pressure head (immersion depth) can be evaluated from $p - T$ phase diagram of ^{4}He or Clausius-Clapeyron equation for the ^{4}He. One guideline is

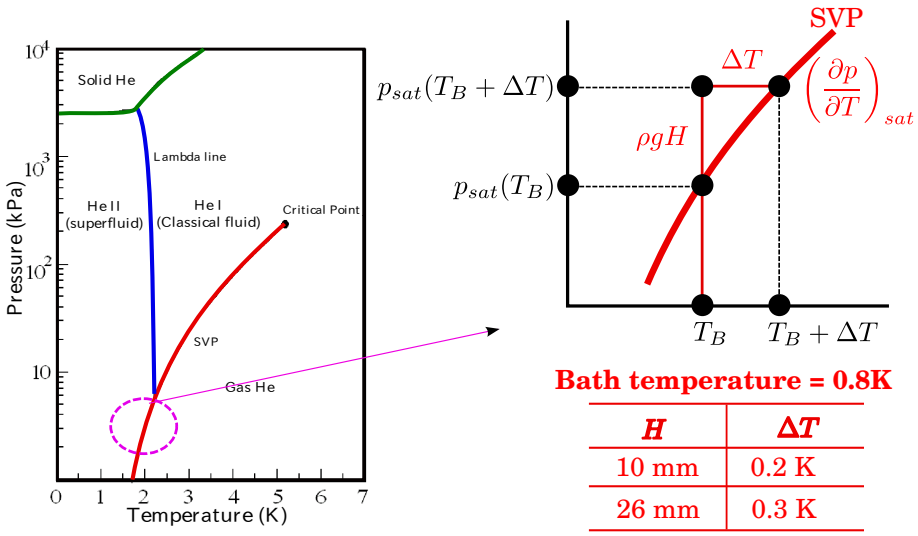

H	*ΔT*
10 mm	0.2 K
26 mm	0.3 K

Figure 1.12: relationship between ρgH and temperature difference, $\Delta T = T_{sat} - T_B$ at saturated temperature of 0.8 K.

to find the hydrostatic pressure head allowing a superfluid helium temperature rise of 0.2 K without film boiling. Figure 1.12 shows the relationship between ρgH and temperature difference, $\Delta T = T_{sat} - T_B$ at saturated temperature of 0.8 K. The gradient of the Saturated Vapor Pressure (SVP) line can be calculated from Clausius-Clapeyron equation described below.

$$\left(\frac{\partial p}{\partial T}\right)_{sat} = \frac{\Delta H}{T \Delta V} \tag{1.10}$$

ΔH and ΔV means the enthalpy and specific volume difference between liquid and gas, respectively. The relationship between hydrostatic pressure head, H, and temperature difference, ΔT is described by following equation.

$$H = \frac{1}{\rho g} \int_{T_B}^{T_B + \Delta T} \left(\frac{\partial p}{\partial T}\right)_{sat} dT \tag{1.11}$$

instead of using equation (1.11), actually required hydrostatic pressure head, H, for getting ΔT can be obtained from HEPAK using following relation.

$$H = \frac{1}{\rho g} \Big[p_{sat}(T_B + \Delta T) - p_{sat}(T_B) \Big] \tag{1.12}$$

According to the calculation using equation (1.12) and HEPAK, required hydrostatic pressure head is 10 mm and 26 mm in order to obatain temperature difference of 0.2 K and 0.3 K.

1.4 Temperature distribution in the UCN guide and UCN bottle

Overall, total heat deposit, Q_{tot}, is removed from 3He-HEX throught the UCN guide pipe. Figure 1.13 shows the schematic model of the heat flow during steady state operation (long term operation). Actually there are two region to be considered.

1. UCN bottle
2. UCN guide pipe

The thermo fluid behaviour of He-II in the UCN bottle is a little bit difficult to evaluate temperature distribution in the 3D-field because of the three dimensional heat deposit. To evaluate temperature distribution in the UCN bottle, instead of one-dimensional Gorter-Mellink equation, we have to conduct three dimensional numerical simulation of full type of two fluid model including superfluid turbulent model by coupling the heat deposit profile. In order to avoid such kind of complex three dimensional simulation on He-II, the temperature increment inside the UCN guide pipe was solved by focusing on the fact that all the heat deposit passes through the UCN guide pipe in the steady state. That is, we only estimate the temperature inside the bottle by extrapolating the temperature distribution inside the UCN guide pipe. If film boiling does not occur in the UCN bottle, He-II temperature in the UCN bottle is almost equal to the highest temperature in the UCN guide pipe. However, the temperature in the UCN bottle may be locally much higher than bath temperature, if film boiling due to the volumetric heating occurs because of the shallow immersion depth (hydrostatic pressure head). If film boiling occurs in the UCN bottle bath, the temperature distribution will be as shown in "axis2" in the figure 1.13. If film boiling phenomanon does not occur in the UCN bottle, temperature distribution along the longitudinal direction will be as shown in the "axis-1" in the figure 1.13.

In order to avoild temperature distribution shown in the axis-2 in the figure 1.13, finite hydrostatic pressure head should be prepared (a little bit large amount of IPHe-II is needed.)

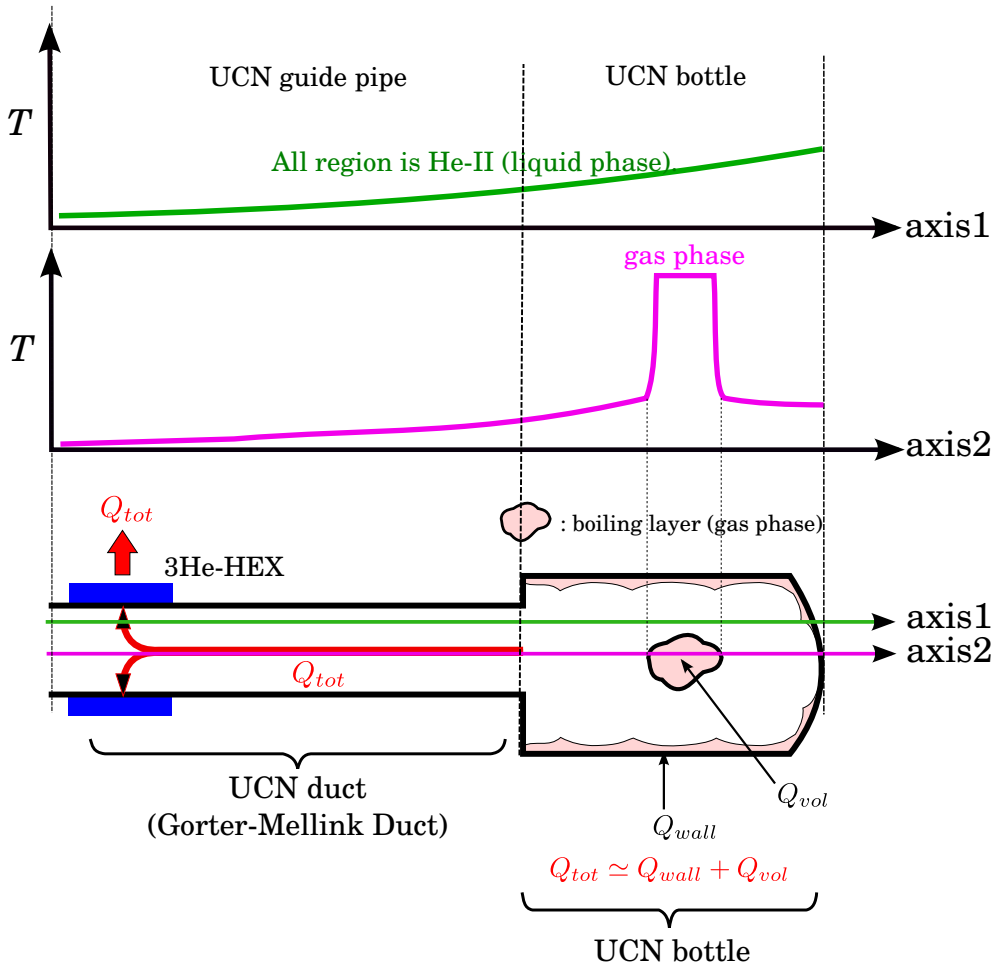

Figure 1.13: Schematic model on the heat flow through the UCN vessel during steady state.

Chapter 2

^{3}He Pumping Duct Design

2.1 Purpose

Previous simulation introduced in the CDR is not realistic simulation because the temperature of the exhaust gas keeps constant for the reduction of the calculation time. As a result, obtained pressure drop from the simulation with such kind of model leads the large pressure drop. Therefore in order to obtain more realistic pressure drop through the ^{3}He pumping duct, we consider the temperature change through the pumping duct and considering the heat transfer effect from the duct wall and static radiation heat transfer by employing energy conservation equation. Main difference between previous simulation and present simulation are listed below.

- previous simulation
  - constant temperature (by considering worst case temp = 70 K)

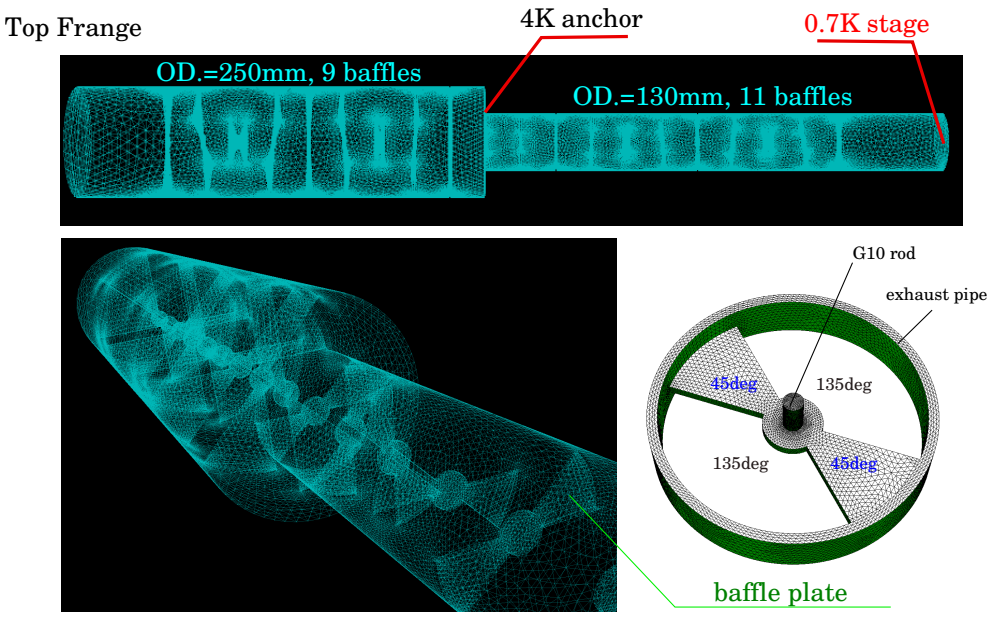

Figure 2.1: ^{3}He pumping duct model with 20 baffle plates.

- not including heat transfer effect through the duct wall and radiation.
- simulation results give us much higher pressure drop than realistic *dp*.
- see CDR chapter 6

- present simulation
  - including heat transfer effect from duct wall, baffle plates.
  - high compressible gas (more than 10 times density difference)
  - More realistic dp will be predicted by applying following scheme.

2.2 System Overall

2.2.1 ^{3}He pumping duct without Hosoyama type HEX

Figure 2.1 shows the ^{3}He pumping duct with 20 baffle plates for the reduction of the static radiation heat load from room temperature region. The detail of this is introduced in the CDR chapter 6.

2.2.2 Hosoyama type HEX

Figure 2.2 shows the Hosoyama type HEX for the precooling of the ^{3}He line. Figure 2.3 is the flow diagram of the UCN cryostat. Hosoyama type HeX shown in the figure 2.2 corresponds to the HEX-2 shown in the figure 2.3. This type of the heat exchanger is needed to get around 1 K of the liquid ^{3}He before passing through the control valve.

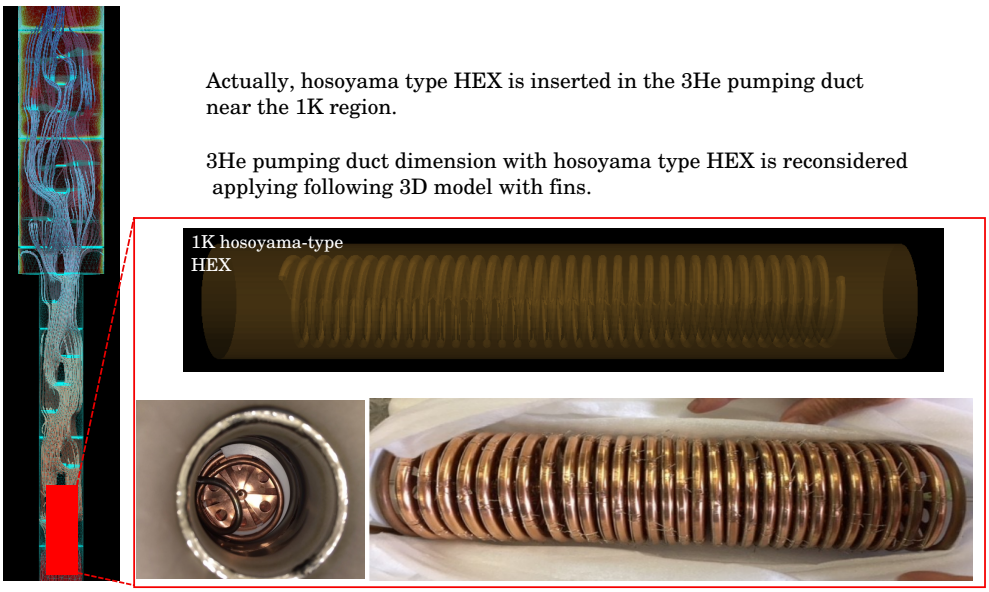

Figure 2.2: Hosoyama type heat exchanger with the spiral shape with a lot of fins.

2.3 Simulation Model

The system equation employed in the previous and present simulation is described as follows.

- previous simulation
  - (incompressible) momentum equation coupled with solenoidal continuity equation.

$$\partial_t \mathbf{u} + (\mathbf{u} \cdot \nabla)\mathbf{u} = -\rho^{-1}\nabla p + \nu^* \nabla \mathbf{u}^1 \tag{2.1}$$

$$\nabla \cdot \mathbf{u} = 0 \tag{2.2}$$

- present simulation

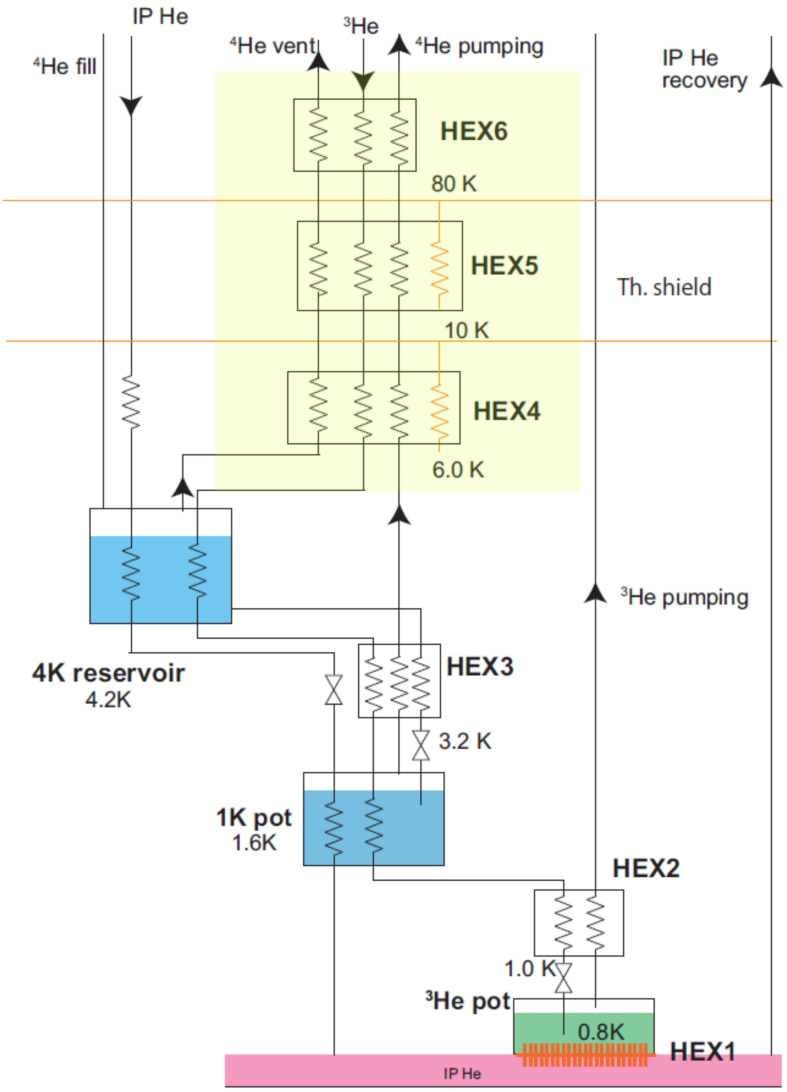

Figure 2.3: flow diagram of the UCN cryostat

[1] ν^* is renormalized viscosity, which can be obtained from LES.

– mass, momentum, energy conservation equation coupled with EOS.[2]

$$\partial_t \mathbf{\Lambda} + \nabla \cdot \mathbf{\Pi} = \mathbf{\Gamma} \tag{2.3}$$

$$pv = z\mathcal{R}T \tag{2.4}$$

$$\mathbf{\Lambda} = \begin{pmatrix} \rho \\ \rho\mathbf{u} \\ \rho E \end{pmatrix}, \quad \mathbf{\Pi} = \begin{pmatrix} \rho\mathbf{u} \\ \rho\mathbf{u}\mathbf{u} - \mathbf{T} \\ \rho E\mathbf{u} - \mathbf{T}\cdot\mathbf{u} + \mathbf{q} \end{pmatrix}, \quad \mathbf{\Gamma} = \begin{pmatrix} 0 \\ \rho\mathbf{f} \\ \rho\mathbf{u}\cdot\mathbf{f} \end{pmatrix} \tag{2.5}$$

In case of present simulation, unlike previous simulation, not only momentum equation but also energy conservation equation including temperature field are solved simultaneously. Therefore the heat transfer effect from the duct wall and radiation heat load can be including in the simulation. Concerning the turbulent treatment, relaminarization from the turbulent to laminar flow may be occurred actually. But in this simulation, whole flow field is regarded as turbulent field to avoid the complexity of simulation. Next subsection shows the calculation example obtained from present simulation scheme. In order to overcome the closure problem of the turbulent field, Large Eddy Simulation (LES) is applied to the present simulation. In addition, in order to reduce the calculation time, Raynolds Averaged Navier Stokes Simulation (RANS) are also conducted.[3] Boundary conditions and other numerical conditions will be introduced later.

2.4 Pressure drop through the duct with a lot of baffles

Figure 2.4 shows the mean temperature and pressure distribution in the ^{3}He pumping duct obtained from LES. Numerical simulation was conducted by applying 10 W heat load which is the worst case. The inlet temperature is 0.7 K with the saturated vapor pressure of 180 Pa.

In the CDR, temperature keeps constant through the pumping duct and its temperature is 70 K. Actually, according to the obtained temperature distribution using present simulation model including energy conservation equation, outlet temperature is lower than 70 K. As a result, total pressure drop through the pumping duct is just sevaral Pa.

2.5 Pressure drop through the Hosoyama type HEX

[2] $\mathbf{T}$, $\mathbf{q}$ and $\mathbf{f}$ is stress tensor, heat flux vector, external force vector, respectively.

[3] Roughly speaking, comparison between LES and RANS is as follows.

- accuracy: LES $\gg$ RANS
- speed: RANS $\gg$ LES

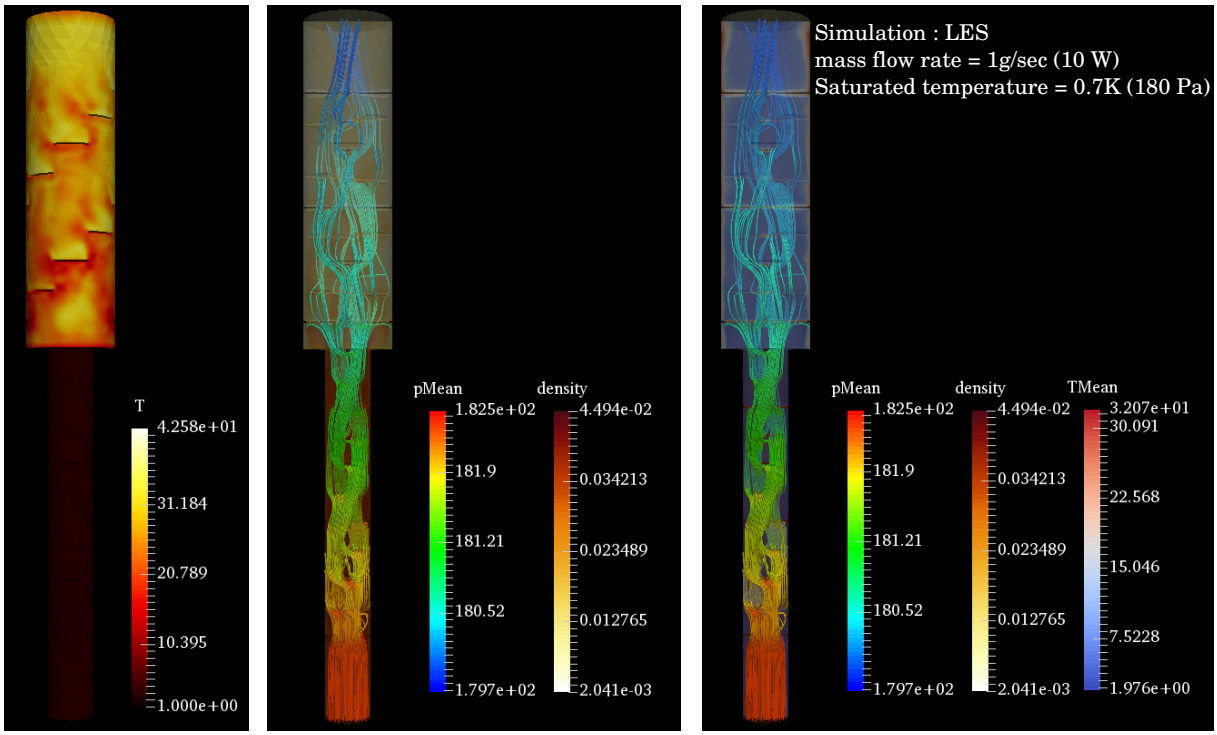

Figure 2.4: Mean temperature and pressure distribution in the ^{3}He pumping duct with 20 baffles.

Result introduced in this subsection is very preliminary.

Figure 2.5 shows the mean pressure and velocity field in the Hosoyama type HEX. **This simulation was performed by applying previous model that the temperature keeps constant through the Hosoyama type HEX. Therefore the energy conservation equation is not solved for this simulation.** And this model has 1/3 times shorter than introduce in the figure 2.2 to reduce the calculation load. The pressure drop obtained from the simulation is 40 Pa with 1/3 shorter model. Therefore the pressure drop for the full scale model may become around 120 Pa. However the previous simulation leads the much larger pressure drop than present simulation model. The pressure drop simulation of the 1/1 scale Hosoyama type HEX is now under calculation by using present simulation model with energy conservation equation with heat transfer effect.

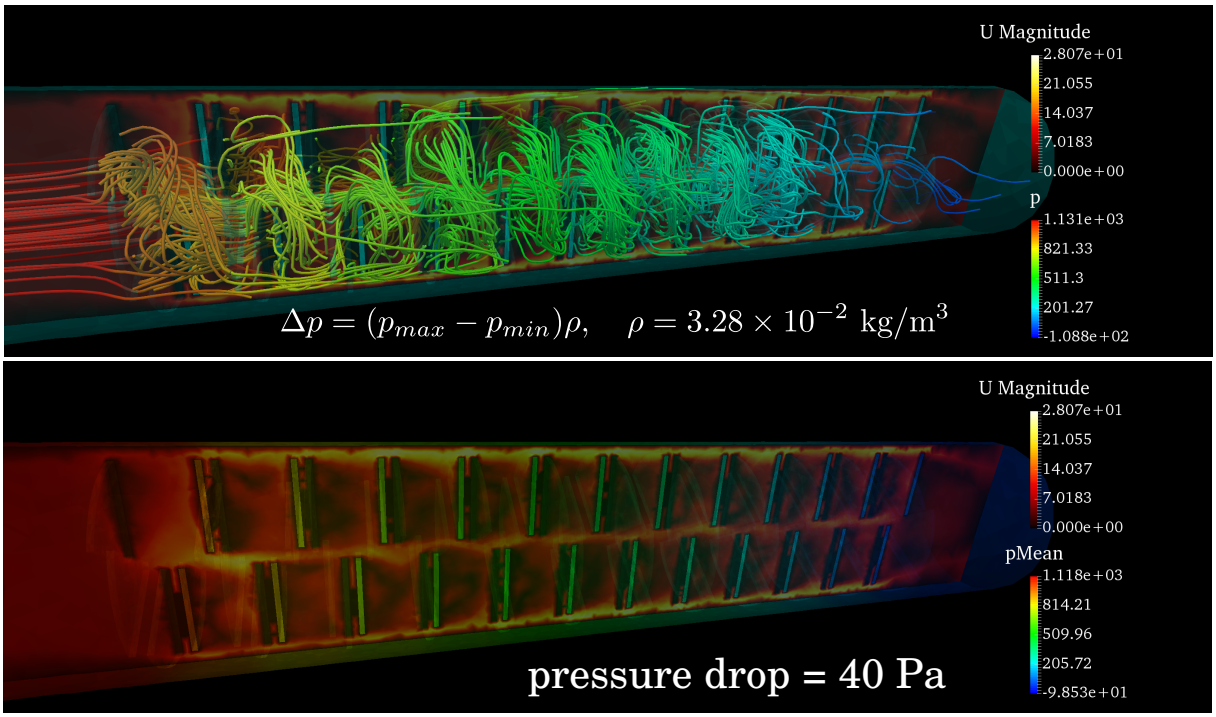

Figure 2.5: Mean temperature and pressure distribution in the ^{3}He pumping duct with 20 baffles.

Chapter 3

Heat Exchanger

3.1 system overall

Chapter 4

Hydrogen and Helium Spill into the Hall during Emergency

4.1 Model

4.1.1 Basic Equations

Following hydrodynamics conservation equations are employed to simulate hydrogen and helium spill into the air.

Mass conservation equation

$$\frac{\partial \rho}{\partial t} + \frac{\partial}{\partial x_\beta}(\rho u_\beta) = 0 \tag{4.1}$$

Momentum equation

$$\rho\left(\frac{\partial u_\alpha}{\partial t} + u_\beta \frac{\partial u_\alpha}{\partial x_\beta}\right) = -\frac{\partial p}{\partial x_\alpha} + \frac{\partial \tau_{\alpha\beta}}{\partial x_\beta} + \rho g \tag{4.2}$$

Energy conservation equation

$$\rho\left(\frac{\partial h}{\partial t} + u_\beta \frac{\partial h}{\partial x_\beta}\right) = -\frac{\partial q_\beta}{\partial x_\beta} + \left(\frac{\partial p}{\partial t} + u_\beta \frac{\partial p}{\partial x_\beta}\right) + \Phi \tag{4.3}$$

species conservation equations

$$\rho\left(\frac{\partial Y_i}{\partial t} + u_\beta \frac{\partial Y_i}{\partial x_\beta}\right) = w_i - \frac{\partial}{\partial x_\beta}(\rho Y_i V_{\beta i}) \tag{4.4}$$

where h：全流体のエンタルピー．h_i：化学種 i のエンタルピー． Y_i：化学種 i の質量分率 $(Y_i = \rho_i / \sum \rho_i)$．$\Phi$：粘性による散逸エネルギー，$w_i$：生成消滅率（ここではゼロ）．$u_\alpha$：全流速ベクトル．$V_{\alpha i}$：化学種 i の拡散速度 $(= \rho_i Y_i V_{\alpha i} = -\rho D_{im} \nabla Y_i)$．すなわち $V_{\alpha i}$ は化学種 i に関する全流体速度を基準とした時の変動速度成分であり，化学種 i の流速ベクトルを $u_{\alpha i}$ とすると，$(u_{\alpha i} = u_\alpha + V_{\alpha i})$．$q_\alpha$：熱流ベクトル．$\tau_{\alpha\beta}$：粘性応力テンソル．$(\alpha, \beta, \gamma) \in \{1, 2, 3\}$：カーテシアン座標系指標．

4.1.2 Viscous Stress Tensor

Viscous stress tensor, $\tau_{\alpha\beta}$, is described as follows.

$$\tau_{\alpha\beta} = \left(\frac{2}{3}\mu - \eta\right) S_{\gamma\gamma}\delta_{\alpha\beta} - 2\mu S_{\alpha\beta}, \quad S_{\alpha\beta} = \frac{1}{2}\left(\frac{\partial u_\alpha}{\partial x_\beta} + \frac{\partial u_\beta}{\partial x_\alpha}\right) \tag{4.5}$$

where μ is viscosity (Pa-sec), η is bulk viscosity (Pa-sec).[1] Actually Stokes assumption is applied to the bulk viscosity. $S_{\alpha\beta}$ is the strain tensor.

4.1.3 Heat and Mass Flux Vector

The general form of the heat flux vector for the multi fluid component can be described as follows by considering Onsager reciprocal relations.

$$q_\beta = -\lambda\frac{\partial T}{\partial x_\beta} + \rho\sum_i h_i Y_i V_{\beta i} + RT\sum_i\sum_j \left(\frac{X_j D_{T,i}}{M_i D_{ij}}\right)(V_{\beta i} - V_{\beta j}) + q_\beta^{rad} \tag{4.6}$$

- $D_{T,i}$：化学種 i の熱拡散係数，λ：平均熱伝導率 (Wilke の法則)
- D_{ij}：化学種 j 中の化学種 i の拡散係数（相互拡散係数）[2].
- X_j：モル分率 ($X_j = C_j/\sum_j C_j = (\rho_j/M_j)/(\sum_j \rho_j/M_j)$, M_i：化学種 i の分子量.
- q_β^{rad}：放射による熱流ベクトル

Dufour 効果と輻射の効果はここでは無視する.

オンサーガーの相反定理のつづき ‥ 物質拡散に関する熱力学的力 ∇X_i

$$\begin{aligned}\nabla X_j = &\sum_j \frac{X_i X_j}{D_{ij}}(V_{\beta j} - V_{\beta i}) + (Y_i - X_i)\left(\frac{\nabla p}{p}\right) + \frac{\rho}{p}\sum_j Y_i Y_j (f_{\beta i} - f_{\beta j}) \\ &+ \sum_j \left\{\left(\frac{X_i X_j}{\rho D_{ij}}\right)\left(\frac{D_{Tj}}{Y_j} - \frac{D_{Ti}}{Y_i}\right)\right\}\left(\frac{\nabla T}{T}\right)\end{aligned} \tag{4.7}$$

♠ 圧力拡散，外力項, 熱拡散 (Soret 効果) を無視.

$$\nabla X_i \simeq \sum_j \frac{X_i X_j}{D_{ij}}(V_{\beta j} - V_{\beta i}) \tag{4.8}$$

かつ $D_{ij} = D_i$ とおくと，化学種保存に関する拡散項は以下の通り簡略化.

$$\rho Y_i V_{\beta i} = -\rho D_i \frac{\partial Y_i}{\partial x_\beta} \tag{4.9}$$

$$-\frac{\partial}{\partial x_\beta}(\rho Y_i V_{\beta i}) = \frac{\partial}{\partial x_\beta}\left(\rho D_i \frac{\partial Y_i}{\partial x_\beta}\right) \tag{4.10}$$

[1] Bulk viscosity, η, is the viscosity effect acting on the volume expansion and contraction. On the contrary, viscosity, μ, means the viscosity effect acting on the shear stress in the flow field.

[2] ここでは空気に関する相互拡散係数

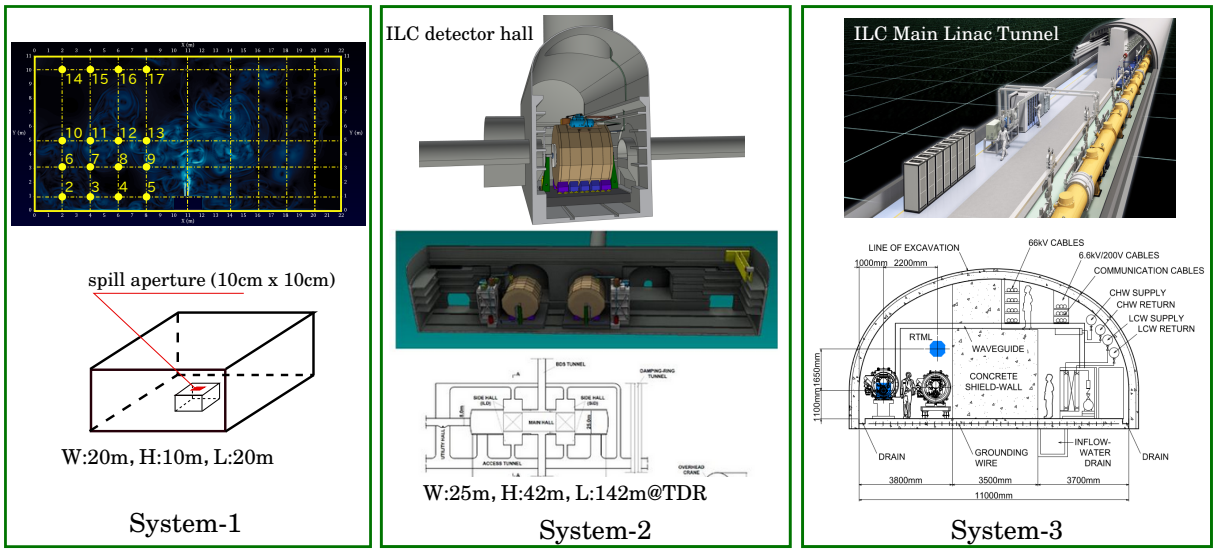

Figure 4.1: Analytical model example.

4.2 Analytical Model Examples

Figure 4.1 shows the analytical model example.

4.3 Simulation Result Examples

4.3.1 Various Gas Discharge Behaviour

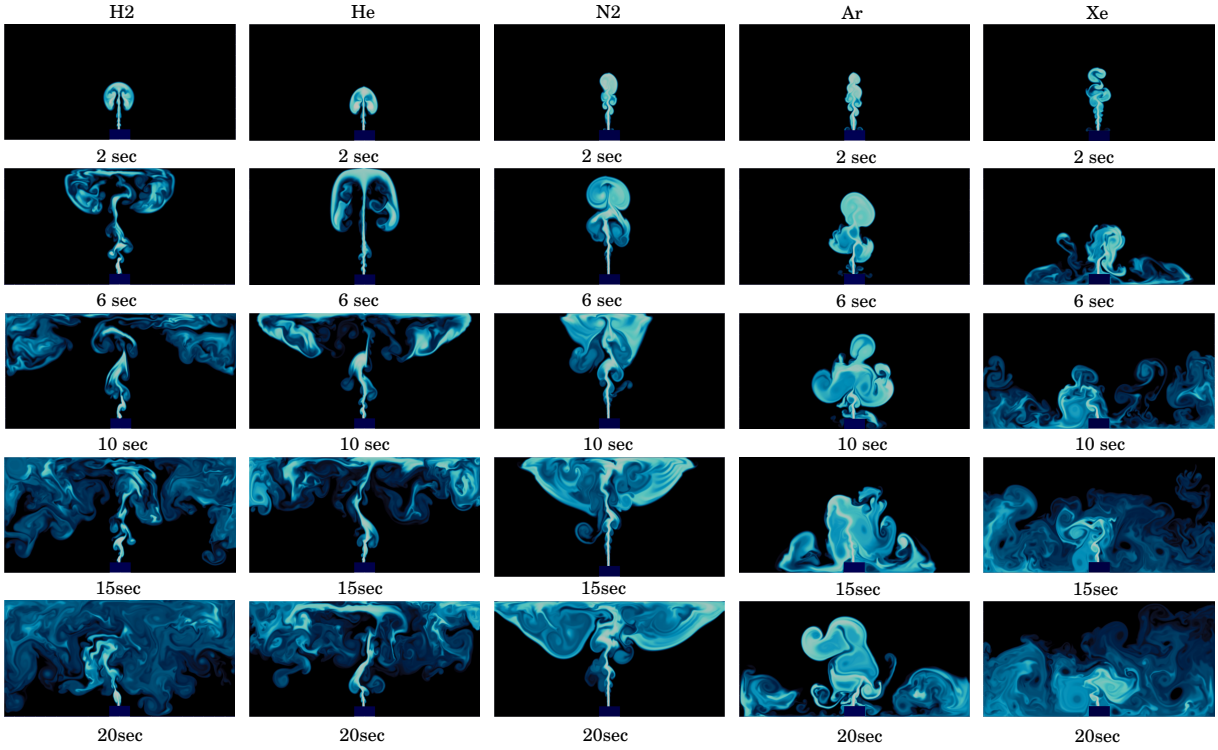

Figure 4.2: Various gas advection diffusion behaviour with temperature of 300 K

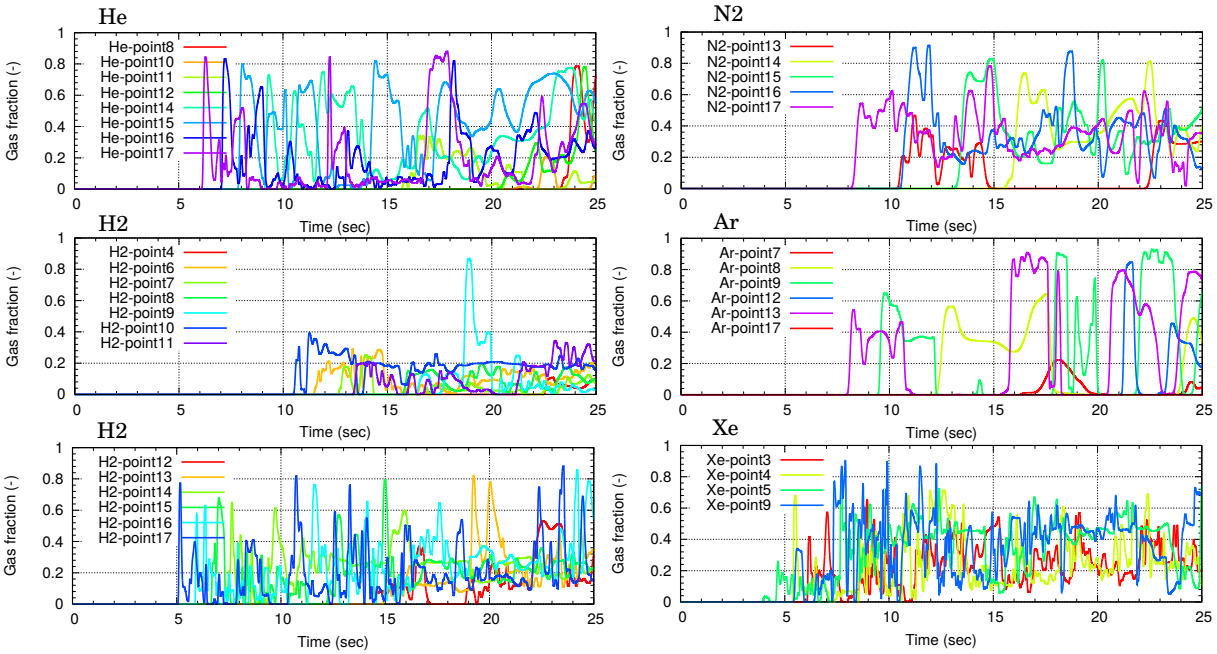

Figure 4.3: Time dependent of the oxygen concentration during the various gas spill into the air.

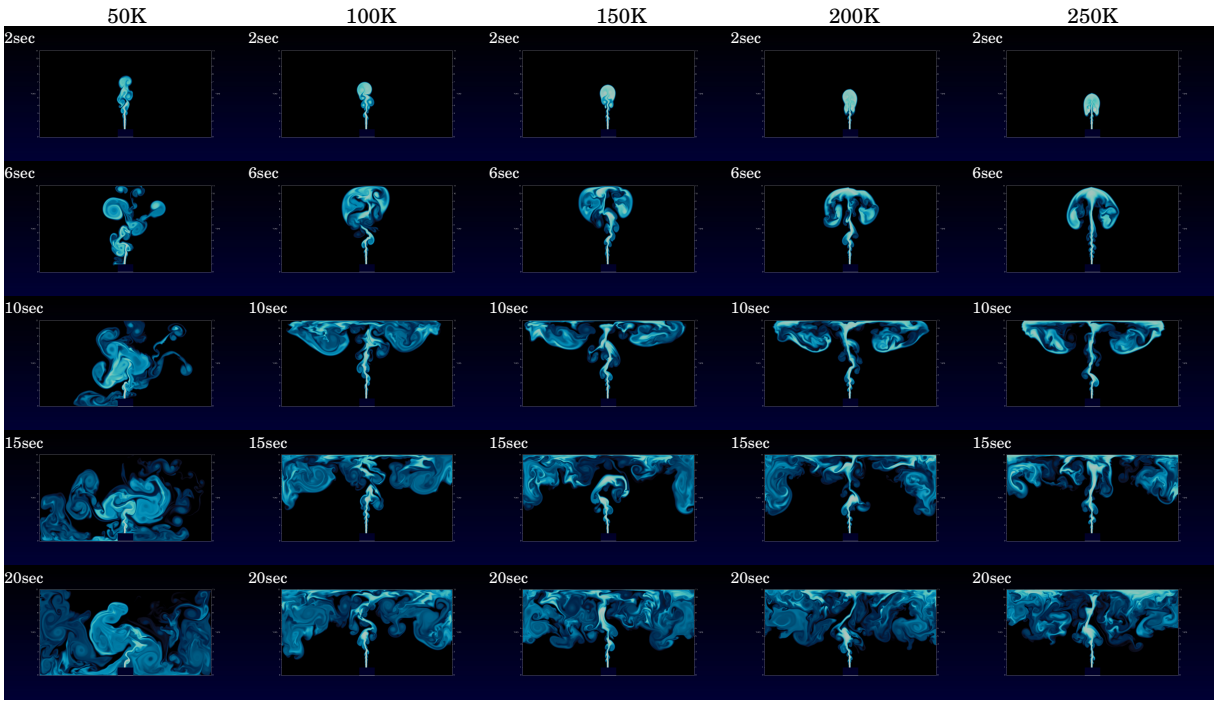

Figure 4.4: Helium gas behaviour for the various spill temperature

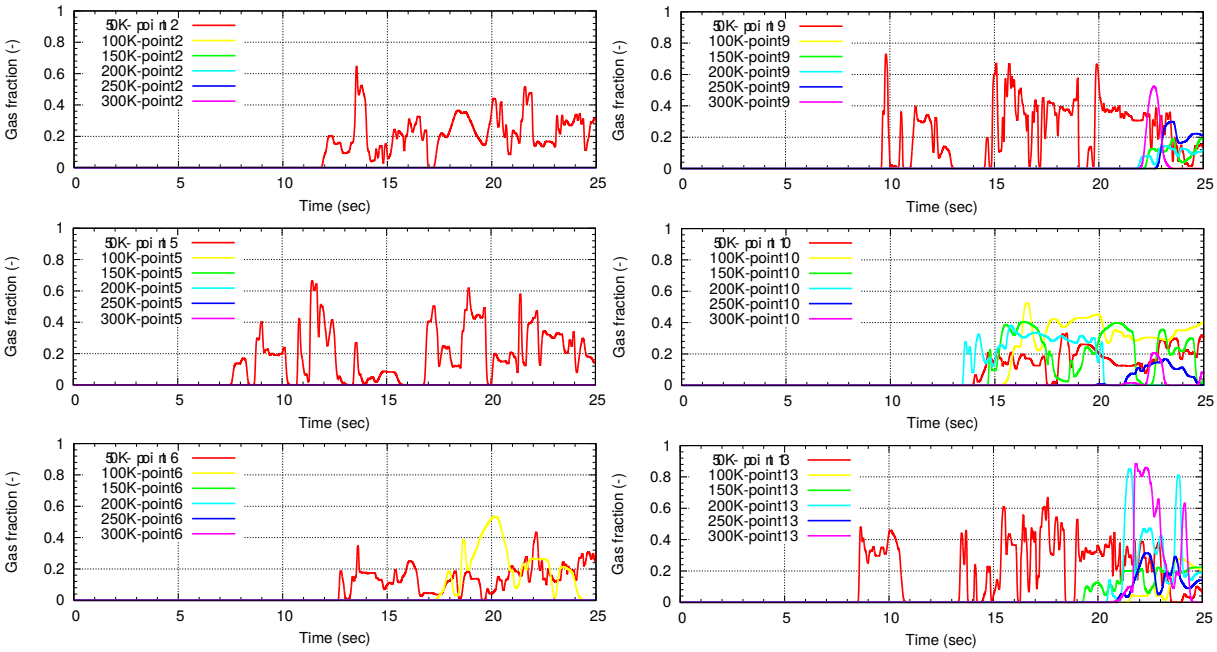

Figure 4.5: Time depnendent of the oxygen concentration for the helium gas behaviour for the various spill temperature

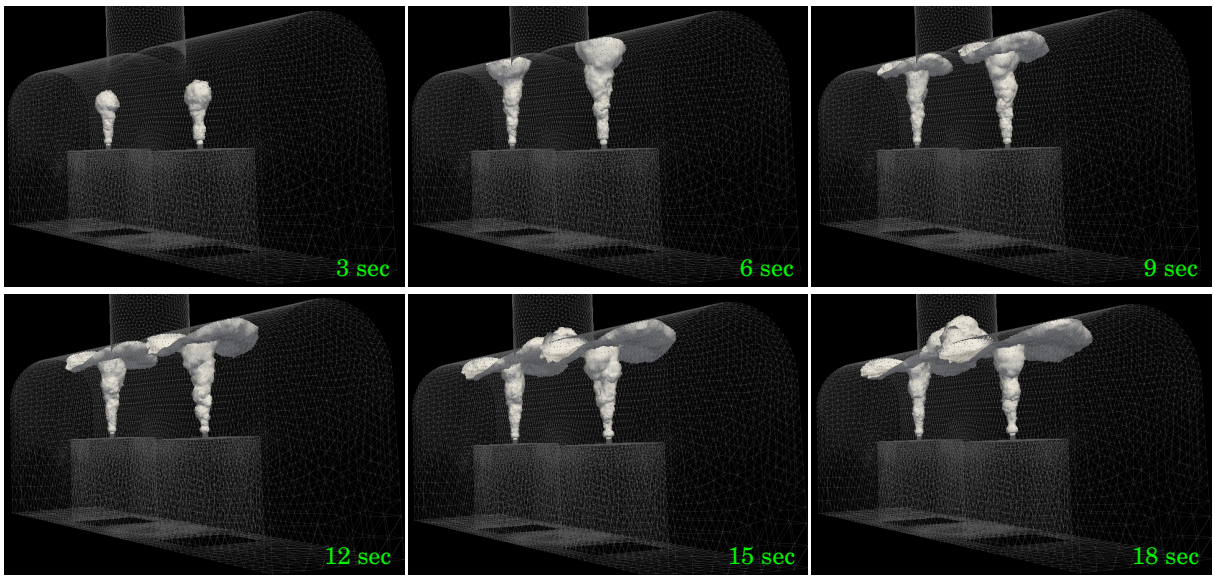

Figure 4.6: Time dependent of helium spill into the ILC detector hall.

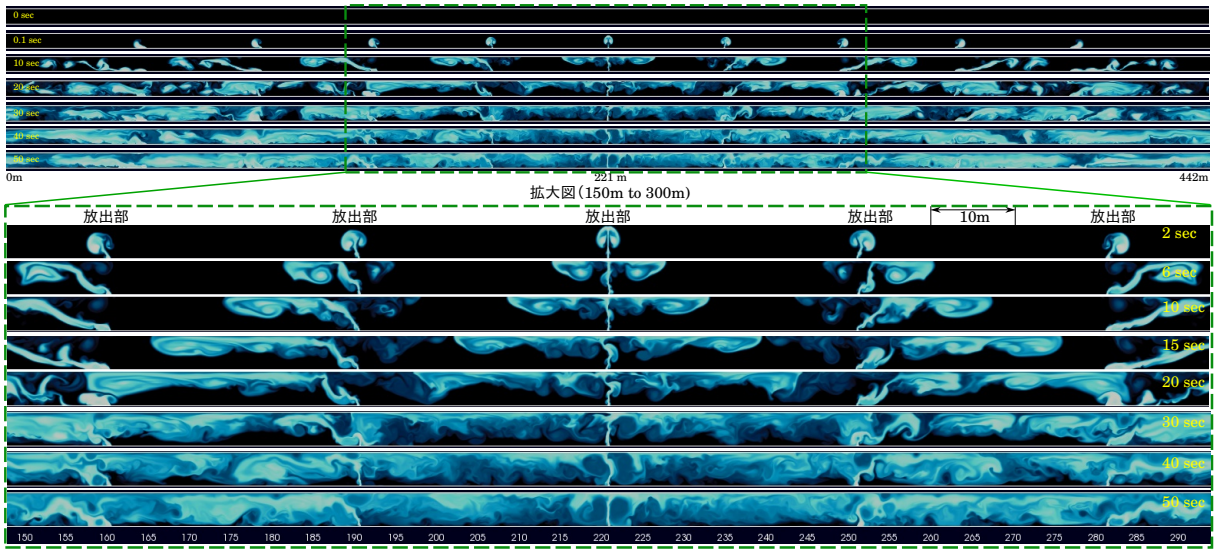

Figure 4.7: Time dependent of helium spill into the ILC accelerator tunnel in the case of a lot of spill points.

Chapter 5

Kapitza Conductance Measurement

Chapter 6

$f(T)^{-1}$ measurement

Bibliography

[1] Maria C. Vlachou, John S. Lioumbas, Thodoris D. Karapantsios, "HEAT TRANSFER ENHANCEMENT IN BOILING OVER MODIFIED SURFACES: A CRITICAL REVIEW", Interfacial Phenomena and Heat Transfer, 3 (4): 341367 (2015)

[2] http://www.me.umn.edu/courses/me4331/FILES/Nukiyama.pdf#search=%27Nukiyama%27s+boiling+curve%27 ···

[3] http://www.iaea.org/inis/collection/NCLCollectionStore/_Public/37/104/37104705.pdf#search=%27%EF%BC%AE%EF%BD%95%EF%BD%8B%EF%BD%89%EF%BD%99%EF%BD%81%EF%BD%8D%EF%BD%81%EF%BC%87%EF%BD%93+boiling+curve%27

[4] Advances in cryogenic engineering , Vol. 25, p374